mathematics

Article

A Radial Basis Scale Conjugate Gradient Deep Neural Network for the Monkeypox Transmission System

Zulqurnain Sabir [1,2,3], Salem Ben Said [1,*] and Juan L. G. Guirao [4,5]

1 Department of Mathematical Sciences, UAE University, Al Ain P.O. Box 15551, United Arab Emirates
2 Department of Computer Science and Mathematics, Lebanese American University, Beirut 11022801, Lebanon
3 Department of Mathematics and Statistics, Hazara University, Mansehra 21120, Pakistan
4 Department of Applied Mathematics and Statistics, Technical University of Cartagena, Hospital de Marina, 30203 Cartagena, Spain
5 Nonlinear Analysis and Applied Mathematics (NAAM)-Research Group, Department of Mathematics, Faculty of Science, King Abdulaziz University, P.O. Box 80203, Jeddah 21589, Saudi Arabia
* Correspondence: salem.bensaid@uaeu.ac.ae

Abstract: The motive of this study is to provide the numerical performances of the monkeypox transmission system (MTS) by applying the novel stochastic procedure based on the radial basis scale conjugate gradient deep neural network (RB-SCGDNN). Twelve and twenty numbers of neurons were taken in the deep neural network process in first and second hidden layers. The MTS dynamics were divided into rodent and human, the human was further categorized into susceptible, infectious, exposed, clinically ill, and recovered, whereas the rodent was classified into susceptible, infected, and exposed. The construction of dataset was provided through the Adams method that was refined further by using the training, validation, and testing process with the statics of 0.15, 0.13 and 0.72. The exactness of the RB-SCGDNN is presented by using the comparison of proposed and reference results, which was further updated through the negligible absolute error and different statistical performances to solve the nonlinear MTS.

Keywords: monkeypox; deep neural networks; nonlinear; radial basis; scale conjugate gradient; hidden layers

MSC: 68T07

check for updates

Citation: Sabir, Z.; Said, S.B.; Guirao, J.L.G. A Radial Basis Scale Conjugate Gradient Deep Neural Network for the Monkeypox Transmission System. *Mathematics* **2023**, *11*, 975. https://doi.org/10.3390/math11040975

Academic Editors: Maria Luz Gandarias, Maria Rosa and Rita Tracinà

Received: 2 January 2023
Revised: 29 January 2023
Accepted: 13 February 2023
Published: 15 February 2023

1. Introduction

Public health professionals are unsure whether monkeypox virus (MV) will offer a new threat despite the coronavirus still being a risk in view of the recent pandemic it already has caused [1,2]. An illness with two DNA viruses, the cowpox, variola and vaccinia, as well as MV, are all family members of the orthopoxvirus [3]. The MV was originally detected in monkeys in the middle of 20th century. The natural form of MV contains rope/tree squirrels, dormice, and Gambian pouched rats [4]. MV severely affected the African regions, particularly the western and central areas [5]. Several epidemiological incidents have been linked to sexual activity, especially in male, gay and bisexual individuals [6–8]. MV can also be spread via sharing bedding or clothing, as well as by being in close contact with scabs, infectious sores, or bodily fluids [9]. Each individual experienced different MV symptoms. Smallpox-like symptoms include a recognizable rash with mild prodromal signals, although they are less severe than smallpox symptoms such as illness, lymphadenopathy, and fever [10]. Patients with this epidemic often experience a dermatitis that starts in the vaginal/perianal parts and could or might not expand to other internal organs [11]. Viral genetic research of swabs were taken from the continental crust of ulceration or blisters, which is the suggested technique for determining the presence of current MV cases [12]. Numerous nations have notified the World Health Organization

(WHO) about MV since the beginning of 2022. According to the WHO, 2103 cases were reported with laboratory diagnosis and one was death registered in the middle of the last year [13,14].

To identify naturally occurring phenomena, a variety of mathematical concepts have been applied using the prey–predator interactions and interspecies communications. The virus can be spread by direct contact with body liquids from sick persons and illnesses [15,16]. Monkeypox is an infectious disease, the treatment for which has not been identified until now. Antiviral drugs, the vaccine immune globulin, and chicken pox vaccination have all been created to protect against the MV. Chickenpox has been eliminated worldwide and its vaccination was not accessible for a long time [17,18]. The virus's trends are uncertain because it has not received much attention previously. Even so, investigators have tried to objectively investigate the behavior of MV and have developed an intricate computational approach [19]. To prevent the spread of illness, infected patients should be kept apart from the public. A design of a nonlinear system was presented to designate the dynamics of the MV [20]. The simulated analysis revealed that a person's immunological status is affected if they sustain an orthopoxvirus sickness. To better explain how illnesses spread and find new therapy modalities, many computer simulations of serious illnesses are currently being investigated [21–23].

The current investigations indicate the numerical solutions of the monkeypox transmission system (MTS) by applying the novel stochastic procedure of radial basis scale conjugate gradient deep neural network (RB-SCGDNN). Twelve and twenty neurons in the first and second hidden layers have been applied to solve the MTS. The stochastic RB-SCGDNN has never been exploited before to solve the mathematical MTS. The numerical stochastic procedures based supervised/unsupervised neural networks have been implemented in various disciplines, e.g., coronavirus system [24], food chain model [25], HIV infectious systems [26], delay mathematical model [27], and differential form of the singular systems [28]. The MTS dynamics were categorized into rodent and human; the rodent was classified into three groups: susceptible, infected, and exposed, while the human was classified into susceptible, infectious, exposed, clinically ill, and recovered. The generic form of nonlinear MTS is shown as [29]:

$$\begin{cases} S'_H(\theta) = \varphi_H - (\lambda_H + \mu_H)S_H(\theta), \\ E'_H(\theta) = \lambda_H S_H(\theta) - (\beta + \mu_H)E_H(\theta), \\ I'_H(\theta) = \beta E_H(\theta) - (\psi + \gamma + \mu_H + \delta_1)I_H(\theta), \\ C'_H(\theta) = \gamma I_H(\theta) - (\rho + \delta_2 + \mu_H)C_H(\theta), \\ R'_H(\theta) = \psi I_H(\theta) + \rho C_H(\theta) - \mu_H R_H(\theta), \\ S'_R(\theta) = \varphi_R - (\lambda_R + \mu_R)S_R(\theta), \\ E'_R(\theta) = -(\varepsilon + \mu_R)E_R(\theta) + \lambda_R S_R(\theta), \\ I'_R(\theta) = \varepsilon E_R(\theta) - \mu_R I_R(\theta). \end{cases} \tag{1}$$

where S_H, E_H, I_H, C_H and R_H present the susceptible, exposed, infectious, clinically ill, and recovered human, while S_R, E_R and I_R indicate the susceptible, exposed, and infectious rodents. φ_R and φ_H are the rodent and human susceptible recruitments, γ shows the clinically ill ratio, μ_H and μ_R represent the natural death rate per capita in humans and rodents, λ_R and λ_H indicate the natural death and infection force, β is the progression rate of illness based on the infection-exposed humans, δ_1 and δ_2 are the transferrable and clinically diseased persons, ρ presents the recovered ratio of clinically ill individuals, ψ is the natural recovered immunity rate and ε is the rate of growing communicable rodents. Some novel features of this work are presented as:

- The stochastic RB-SCGDNN is presented to find the precise solutions of the nonlinear dynamics of MTS.

- The solutions of MTS are obtained through the RB-SCGDNN by taking twelve and twenty neurons in the hidden layers.
- A dataset is provided through the Adams method that is refined further by using the training, validation, and testing process with the statics of 0.15, 0.13, and 0.72.
- The exactness of RB-SCGDNN is presented by comparison of reference and achieved results, which is further validated using the negligible values of the absolute error together with different statistical measures to solve the MTS.

The rest of the paper is summarized as: the RB-SCGDNN based methodology is shown in Section 2. Discussions of the results is presented in Section 3 and conclusions are reported in Section 4.

2. Methodology

In this section, a methodology based on the stochastic operators is presented to solve the mathematical form of the nonlinear MTS. The mathematical and graphical procedures based on the multi-layer structures are also presented.

2.1. RB-SCGDNN Procedures

The mathematical RB-SCGDNN is presented with twelve and twenty neurons in the 1st and 2nd hidden layers, which is given as:

$$\begin{bmatrix} p_1 \\ p_2 \\ p_3 \\ \cdot \\ \cdot \\ \cdot \\ p_{12} \end{bmatrix} = \Lambda\left(\begin{bmatrix} w_{1,1} \\ w_{1,2} \\ w_{1,3} \\ \cdot \\ \cdot \\ \cdot \\ w_{1,12} \end{bmatrix}[\theta] + \begin{bmatrix} q_{1,1} \\ q_{1,2} \\ q_{1,3} \\ \cdot \\ \cdot \\ \cdot \\ q_{1,12} \end{bmatrix}\right) \tag{2}$$

$$\begin{bmatrix} s_1 \\ s_2 \\ s_3 \\ \cdot \\ \cdot \\ \cdot \\ s_{20} \end{bmatrix} = \Lambda\left(\begin{bmatrix} \psi_{1,1} & \psi_{2,1} & \psi_{3,1} & \psi_{4,1} & \cdot & \cdot & w_{12,1} \\ \psi_{1,2} & \psi_{2,2} & \psi_{3,2} & \psi_{4,2} & \cdot & \cdot & w_{12,2} \\ \psi_{1,3} & \psi_{2,3} & \psi_{3,3} & \psi_{4,3} & \cdot & \cdot & w_{12,3} \\ \cdot & \cdot & \cdot & \cdot & \cdot & \cdot & \cdot \\ \cdot & \cdot & \cdot & \cdot & \cdot & \cdot & \cdot \\ \cdot & \cdot & \cdot & \cdot & \cdot & \cdot & \cdot \\ \psi_{1,20} & \psi_{2,20} & \psi_{3,20} & \psi_{4,20} & \cdot & \cdot & w_{12,20} \end{bmatrix}\begin{bmatrix} p_1 \\ p_2 \\ p_3 \\ \cdot \\ \cdot \\ \cdot \\ p_{12} \end{bmatrix} + \begin{bmatrix} q_{2,1} \\ q_{2,2} \\ q_{2,3} \\ \cdot \\ \cdot \\ \cdot \\ q_{2,20} \end{bmatrix}\right) \tag{3}$$

$$\begin{bmatrix} S_H(\theta) \\ E_H(\theta) \\ I_H(\theta) \\ C_H(\theta) \\ R_H(\theta) \\ S_R(\theta) \\ E_R(\theta) \\ I_R(\theta) \end{bmatrix} = \Lambda\left(\begin{bmatrix} \omega_{1,1} & \omega_{2,1} & \omega_{3,1} & \cdot & \cdot & \cdot & \omega_{20,1} \\ \omega_{1,2} & \omega_{2,2} & \omega_{3,2} & \cdot & \cdot & \cdot & \omega_{20,2} \\ \omega_{1,3} & \omega_{2,3} & \omega_{3,3} & \cdot & \cdot & \cdot & \omega_{20,3} \\ \omega_{1,4} & \omega_{2,4} & \omega_{3,4} & \cdot & \cdot & \cdot & \omega_{20,4} \\ \omega_{1,5} & \omega_{2,5} & \omega_{3,5} & \cdot & \cdot & \cdot & \omega_{20,5} \\ \omega_{1,6} & \omega_{2,6} & \omega_{3,6} & \cdot & \cdot & \cdot & \omega_{20,6} \\ \omega_{1,7} & \omega_{2,7} & \omega_{3,7} & \cdot & \cdot & \cdot & \omega_{20,7} \\ \omega_{1,8} & \omega_{2,8} & \omega_{3,8} & \cdot & \cdot & \cdot & \omega_{20,8} \end{bmatrix}\begin{bmatrix} s_1 \\ s_2 \\ s_3 \\ \cdot \\ \cdot \\ \cdot \\ s_{20} \end{bmatrix} + \begin{bmatrix} q_{3,1} \\ q_{3,2} \\ q_{3,3} \\ q_{3,4} \\ q_{3,5} \\ q_{3,6} \\ q_{3,7} \\ q_{3,8} \end{bmatrix}\right), \tag{4}$$

where w and ψ are the weight vectors in first and second layer, while ω is the output layer weights. p and s indicate the layers 1 and 2 along with output layers. q shows the bias vector and Λ is the activation function, which is taken as radial basis, which is mathematically given as:

$$\Lambda = \exp(-f^2), \text{ where } f = \sum_{i=1}^{r}(w_i\theta_i) + q, \tag{5}$$

where r presents the neurons. Figure 1 shows the mathematical form of MTS and multi-layers construction together with the accomplished results. Figure 2 shows the procedure of multi-layers along with single and multiple hidden layers by taking twelve and twenty neurons.

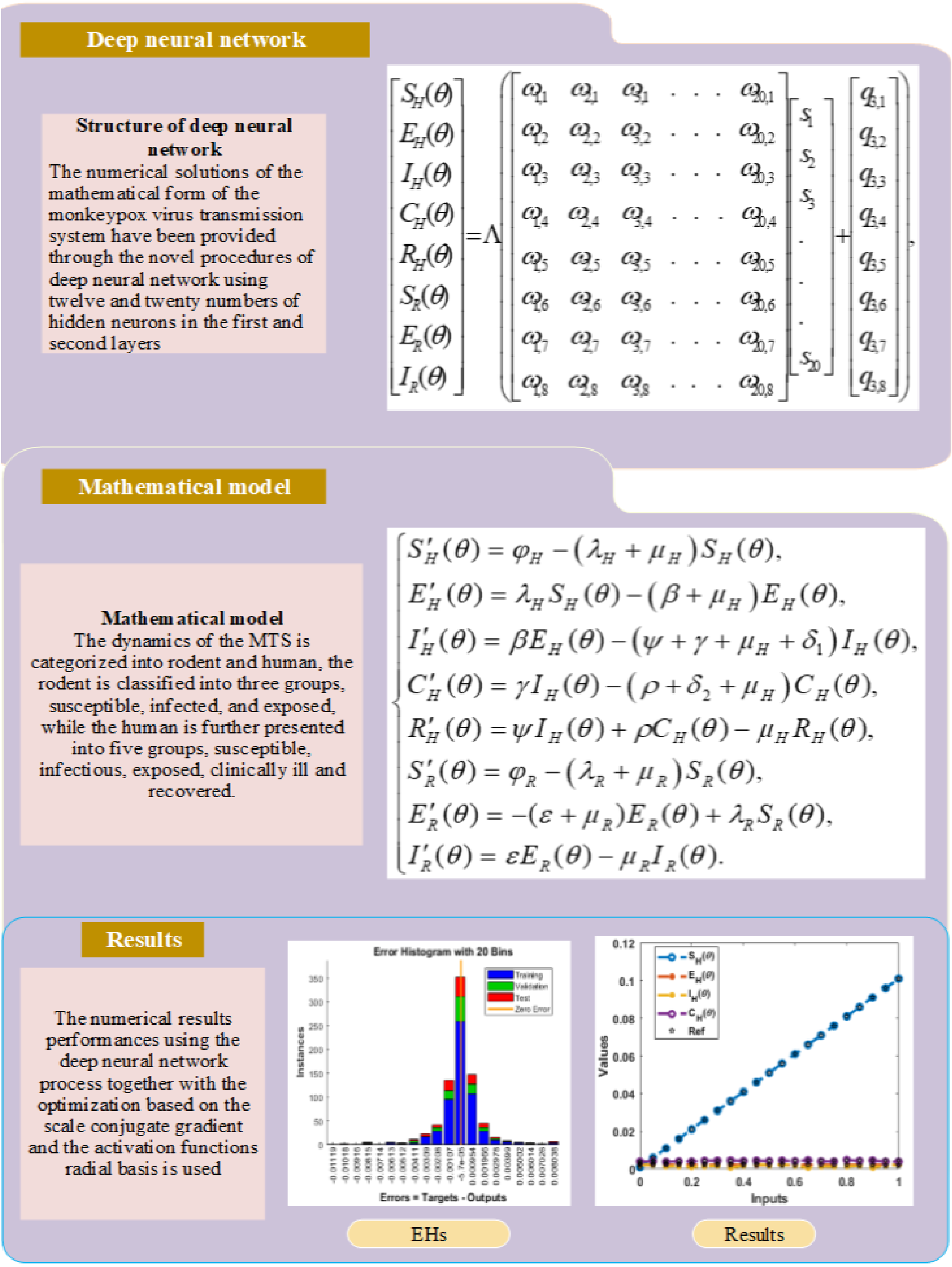

Figure 1. A deep neural network process, mathematical formulations, and assessment of outcomes for the MTS.

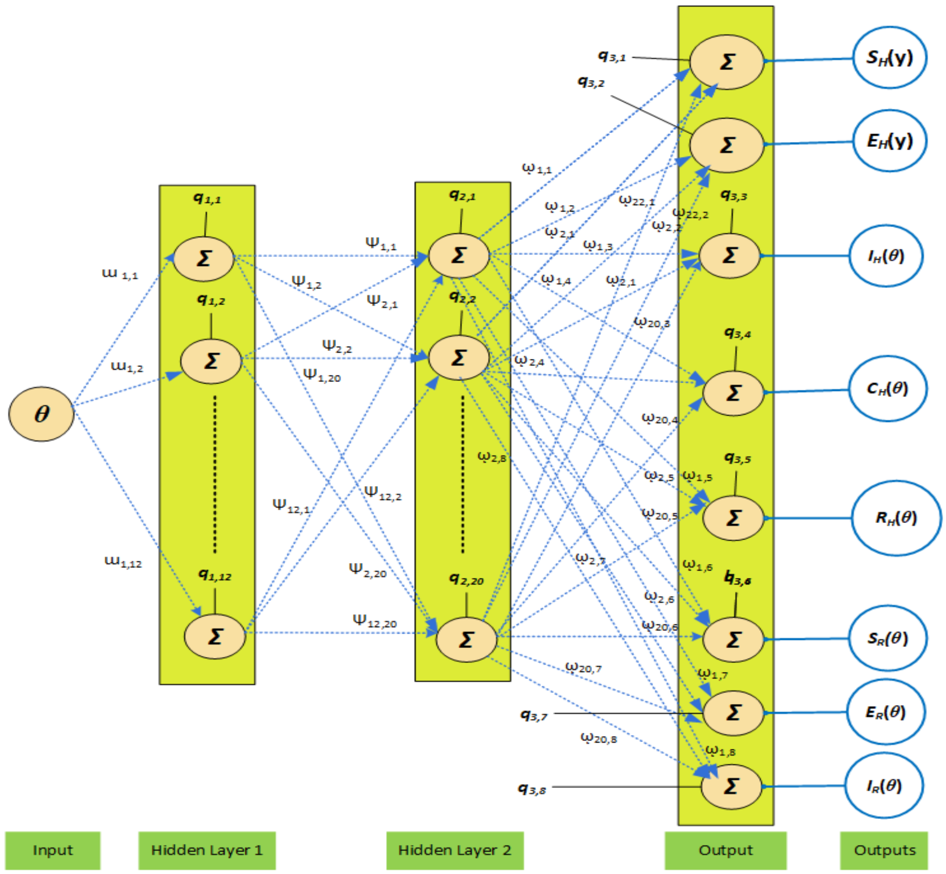

Figure 2. A multilayers procedure for the nonlinear MTS.

The deep neural network by taking twelve and twenty neurons using the 1st and 2nd layers, the 850 selected epochs, radial basis activation function, and the performances have been tested based on mean square error (MSE) and scale conjugate gradient was used in the process of optimization, which is presented in Figure 3.

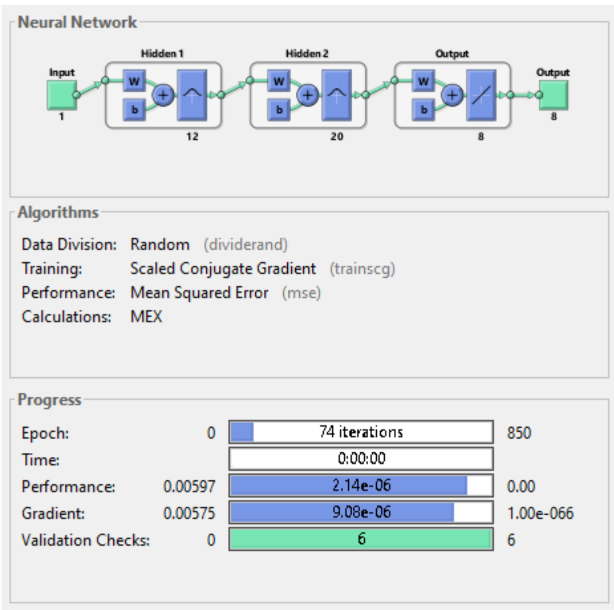

(**a**)

Figure 3. *Cont.*

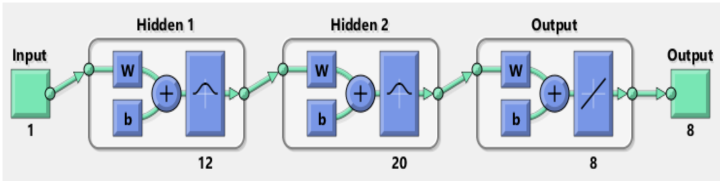

(**b**)

Figure 3. A neural network training performance, an input, couple hidden and output layers for solving the nonlinear dynamics of the MTS. (**a**) A neural network training performance, (**b**) An input, couple hidden and output layers to solve the MTS.

The significant performances to generalize the procedure are presented by applying the Adam numerical solver, whereas the other procedures were executed using the default setting of the parameters in order to produce the dataset. The artificial intelligence aptitudes using the supervised SCGNNs process were accomplished with best indices cooperation, with complexity, overfitting/underfitting, and premature convergence. Moreover, the adjustment of these parameters was approved after comprehensive simulation investigations, experience, and minor variations in the setting. The parameter setting of the SCGNNs method is given in Table 1, accompanied by the slight modification, disparity, and change, which could have caused the poor performance (premature convergence). Hence, these parameter settings were integrated with general consideration for the numerical investigations.

Table 1. Parameter adjustment for the SCGNNs approach.

Index	Settings
Hidden neurons in the first layer	12
Hidden neurons in the second layer	20
Fitness goal (MSE)	0
Maximum Mu values	10^8
Maximum Epochs	850
Minimum values of the gradient	10^{-7}
Increasing Mu performances	10
Decreeing Mu measures	0.2
Training statics	0.15
Testing data	0.72
Validation data	0.13
Samples selection	Random
Generation of dataset	Adam method
Adam method execution and stoppage standards	Default

2.2. *Scale Conjugate Gradient (SCG)*

Moller developed the SCG, which belongs to the family of conjugate gradient algorithms and was widely implemented in the supervised learning for feedforward neural networks [30]. The conjugate gradient is a mathematical scheme, which is applied in the process of optimization whether the system is linear or nonlinear. SCG is normally an iterative method and implemented as a direct search scheme to obtain the numerical results. SCG is an exceptionally straightforward formula for calculating the completely different direction vector. In recent years, SCG has been applied in the number of applications, some of them are image restoration [31], motion control systems [32], inverse scattering problems [33], nonlinear monotone operator models with applications [34], portfolio selection [35], economic and environmental models [36], mild steel turning operation [37], and partial differential models [38].

3. Results and Discussion

The numerical representations for solving three cases based on the rate of human natural death were $\mu_H = 0.000303$, $\mu_H = 0.000202$ and $\mu_H = 0.000101$, while the other parameter values were $\phi_R = 0.2$, $\phi_H = 0.1$, $\psi = 0.088366$, $\mu_H = 0.000303$, $\mu_R = 0.002$, $\varepsilon = 0.1$, $\rho = 0.036246$, $\beta = 0.016744$, $\delta_1 = 0.003286$, $\gamma = 0.5$, $\lambda_H = 0.000202$, $\lambda_R = 0.00404$, $\delta_2 = 0.055487$ and $\sigma = 0.012458$ including initial conditions 0.01, 0.02, 0.03, 0.04, 0.05, 0.1, 0.2, and 0.3 given as [29]:

A procedure based on the stochastic RB-SCGDNN scheme was provided for the numerical solutions of the nonlinear dynamics of MTS. The structure of the first and second hidden layers was provided by taking twelve and twenty number of neurons. Figure 4 indicates the illustrations of the optimal training and transition of state (ToS) by applying the process of deep neural network for solving the nonlinear form of MTS. A total of 850 epochs, an activation radial basis function, and SCG were taken for the purpose of optimization for each case of MTS. MSE using the test, train, and authentication performances are illustrated in Figure 4, which is authenticated as 4.0020×10^{-6}, 1.4172×10^{-5} and 1.0610×10^{-5} at epochs 74, 61, and 38. Figure 4 represents the sum squared, gradient, num parameter, Mu, and substantiation forms. The gradient values are given as 9.0831×10^{-6}, 6.1865×10^{-6} and 7.6674×10^{-6}. Figure 5 shows the fitness function using the test outputs/targets, error, training outputs/targets, and fitness for MTS. Figure 6 authenticates the error histograms (EHs) for the MTS using the deep neural network, activation radial basis function, and SCG optimization. The EHs values for each case of the MTS are illustrated as 5.7×10^{-5}, 3.5×10^{-4}, and 1.08×10^{-4}. The clear performances of the testing dataset are observable; however, the errors performances based on the datasets of training and validation are not clearly noticeable because of the small proportion. The linear tendency of zero-line error presents the proposed results, which were performed closer to reference of the optimal outcomes. Therefore, the point data based on validation/testing is not so clear. The regression (Reg) measures are shown in Figure 7 to signify the numerical representations of the nonlinear MTS are presented as one, which shows a perfect model. R values present the coefficient of correlation, which was applied together with MSE measures of the artificial neural networks. The values of R exist between -1 and +1, while, if the values of R are closer to positive one, the performances of high network along with positive form of the linear relationship can be accomplished. The bias values of the neurons and weights are settled during the process of training until the system learns the correlation performances between the variables based on input and output, i.e., until the minimum values of MSE are obtained. The results of MSE using the test/train performances of the MTS are presented in Table 2.

Table 2. MSE measures using the RB-SCGDNN scheme for the nonlinear MTS.

Case	MSE			Performance	Gradient	Epoch
	Train	Validation	Test			
1	2.41×10^{-6}	4.00×10^{-6}	8.62×10^{-6}	2.14×10^{-6}	9.08×10^{-6}	74
2	2.69×10^{-6}	1.41×10^{-5}	1.49×10^{-5}	2.34×10^{-6}	6.19×10^{-6}	61
3	3.14×10^{-6}	1.06×10^{-5}	1.90×10^{-5}	2.46×10^{-6}	7.57×10^{-6}	38

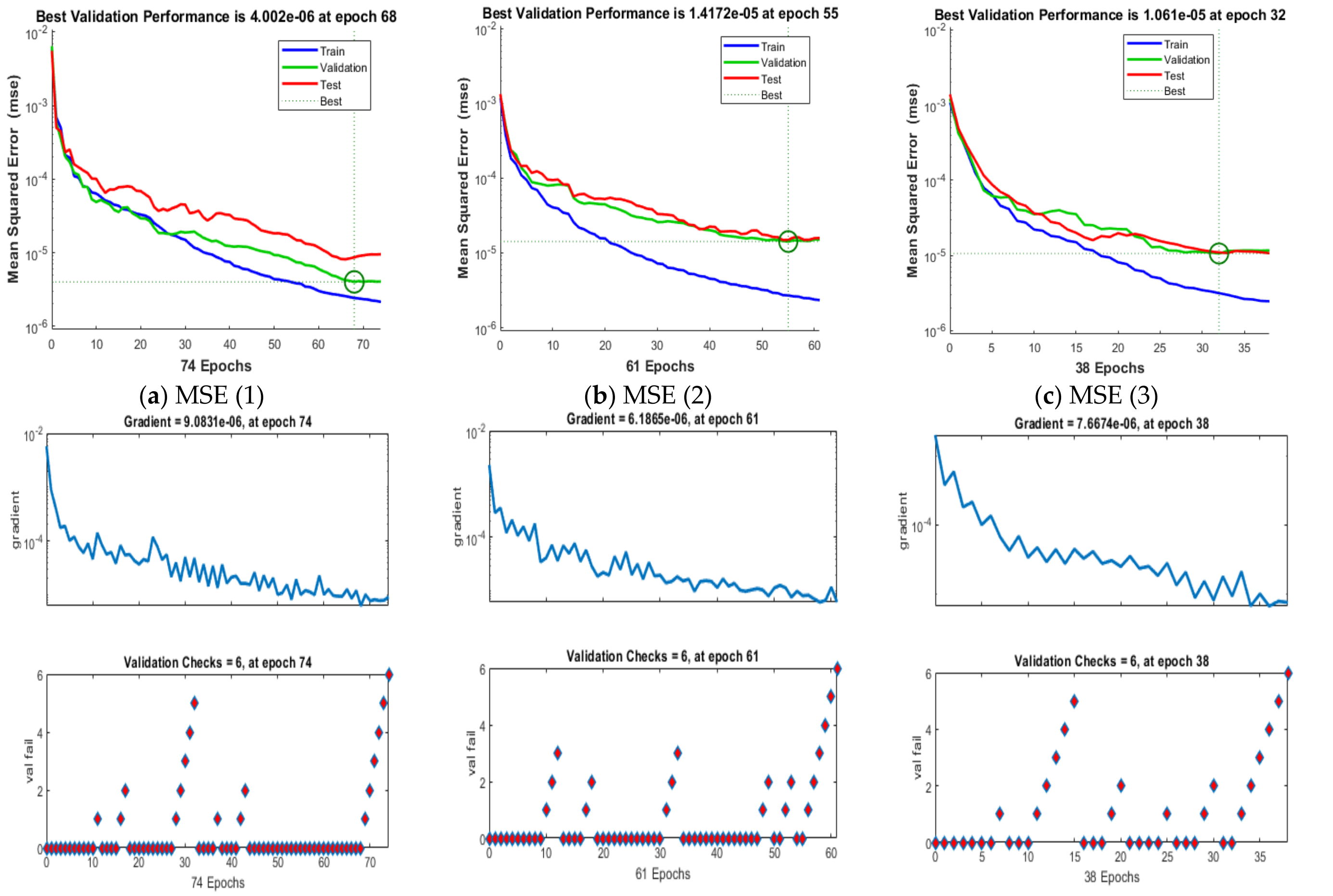

(**a**) MSE (1) (**b**) MSE (2) (**c**) MSE (3)

(**d**) ToS (1) (**e**) ToS (2) (**f**) ToS (3)

Figure 4. Optimal training and ToS for solving the nonlinear dynamics of MTS.

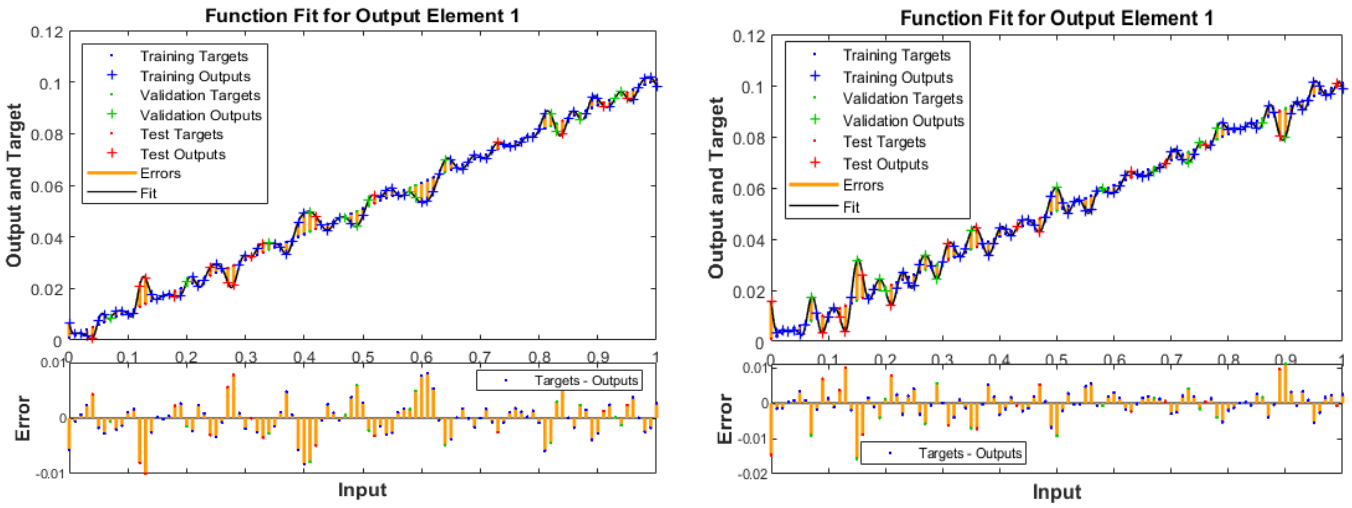

(**a**) Fitness (1) (**b**) Fitness (2)

Figure 5. *Cont.*

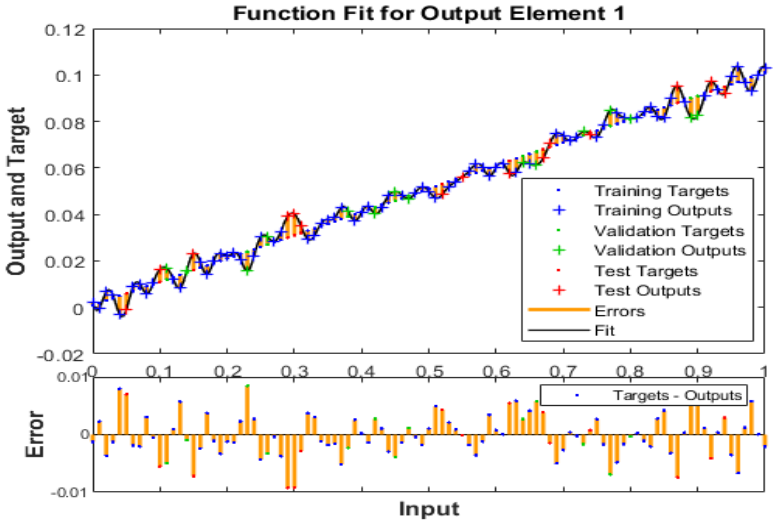

(**c**) Fitness (3)

Figure 5. Function fitness for solving the nonlinear dynamics of MTS.

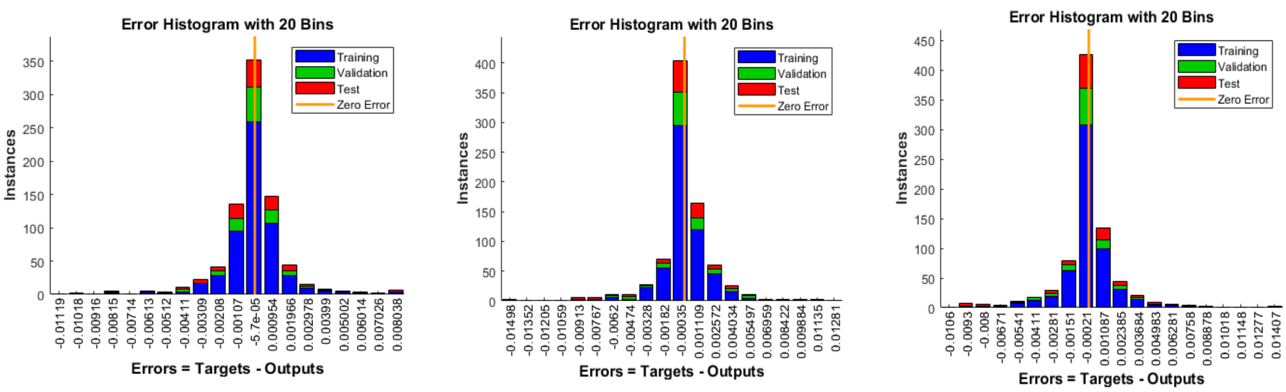

(**a**) EHs (1) (**b**) EHs (2) (**c**) EHs (3)

Figure 6. The performances of EHs for each case the nonlinear dynamics of MTS.

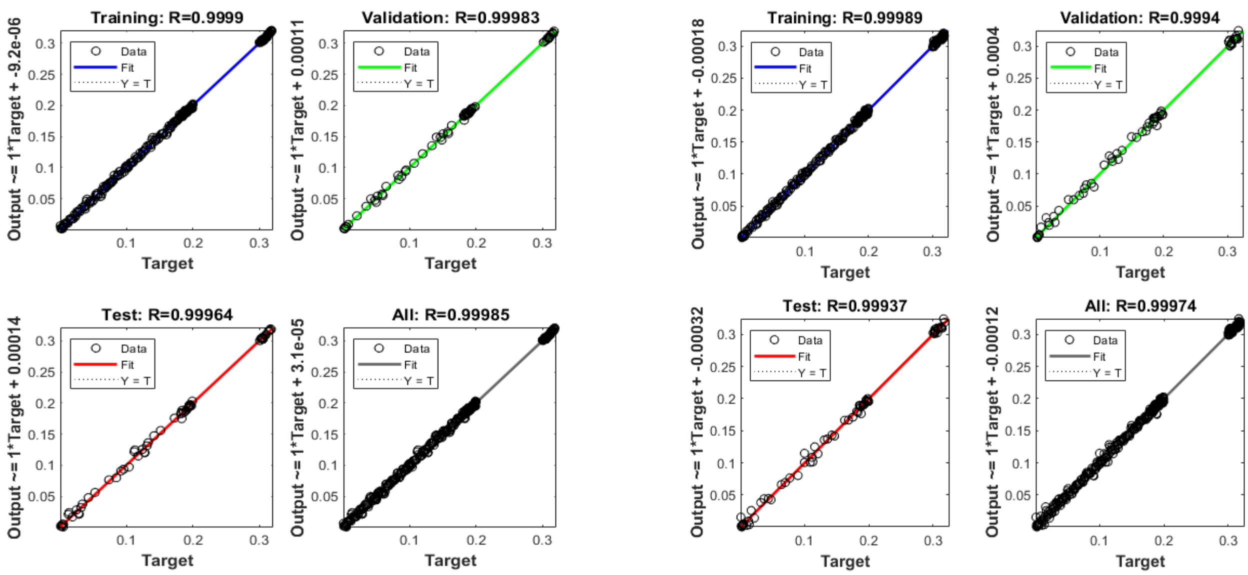

(**a**) Reg. (1) (**b**) Reg. (2)

Figure 7. *Cont.*

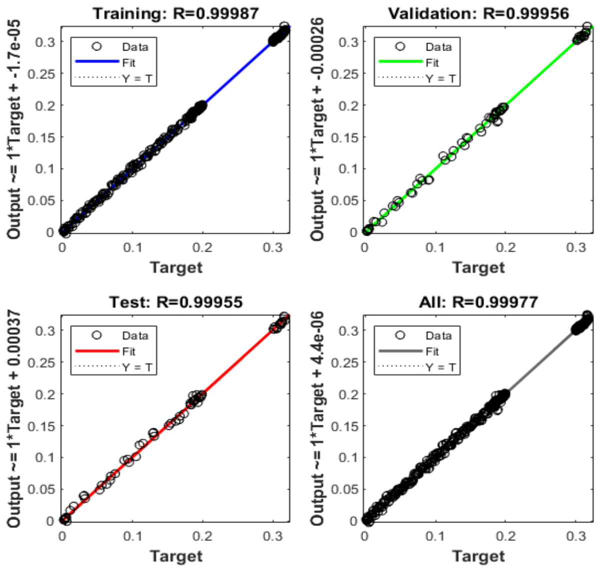

(**c**) Reg. (3)

Figure 7. Reg performances for each case of the MTS.

The comparison performances of each dynamic of nonlinear MTS are presented in Figure 8. The overlapping of the obtained and reference results was accomplished for each dynamic of the MTS, which represents the correctness of the stochastic RB-SCGDNN scheme.

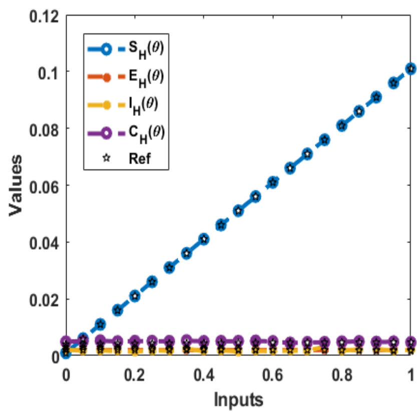

(**a**) Result comparison (1)

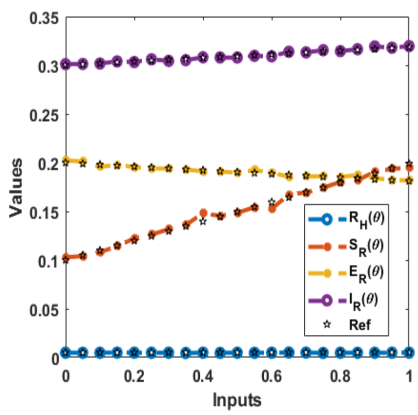

(**b**) Result comparison (1)

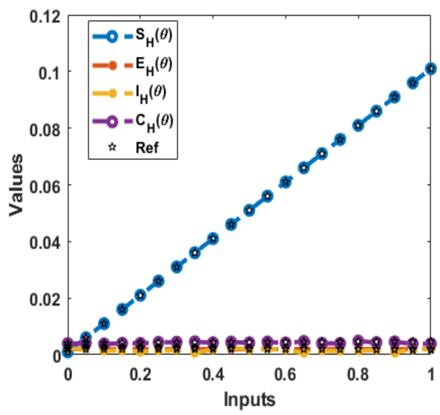

(**c**) Result comparison (2)

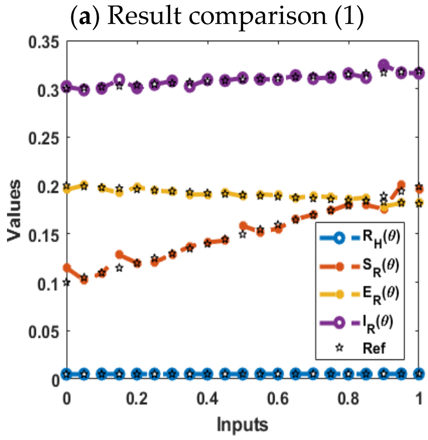

(**d**) Result comparison (2)

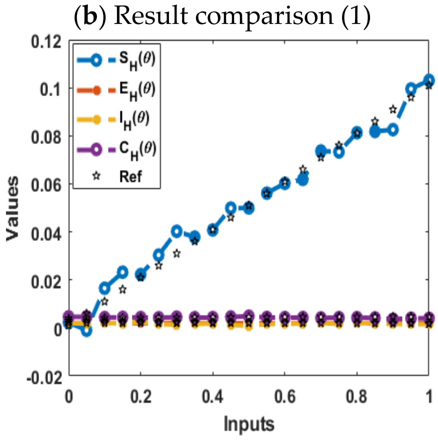

(**e**) Result comparison (3)

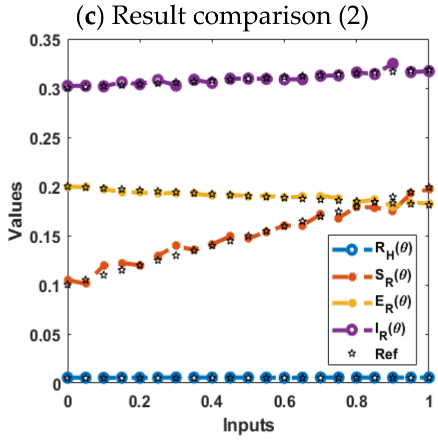

(**f**) Result comparison (3)

Figure 8. Result comparisons for each class of the nonlinear dynamics of the MTS.

AE performances for solving the classes $S_H(\theta)$, $E_H(\theta)$, $I_H(\theta)$, $C_H(\theta)$, $R_H(\theta)$, $S_R(\theta)$, $E_R(\theta)$, and $I_R(\theta)$ of nonlinear MTS are presented in Table 3. These negligible AE performances authenticate the correctness of the RB-SCGDNN scheme.

Table 3. AE for each category of the nonlinear MTS.

θ	**Absolute Error**										
	0	**0.1**	**0.2**	**0.3**	**0.4**	**0.5**	**0.6**	**0.7**	**0.8**	**0.9**	**1**
	6×10^{-3}	1×10^{-3}	1×10^{-3}	2×10^{-3}	8×10^{-3}	3×10^{-3}	8×10^{-3}	3×10^{-5}	8×10^{-4}	3×10^{-3}	3×10^{-3}
$S_H(\theta)$	1×10^{-2}	1×10^{-3}	1×10^{-3}	7×10^{-6}	3×10^{-3}	9×10^{-3}	3×10^{-3}	3×10^{-3}	2×10^{-3}	1×10^{-2}	2×10^{-3}
	1×10^{-3}	6×10^{-3}	1×10^{-3}	9×10^{-3}	2×10^{-4}	1×10^{-3}	8×10^{-4}	3×10^{-3}	3×10^{-4}	8×10^{-3}	2×10^{-3}
	2×10^{-5}	2×10^{-5}	2×10^{-5}	1×10^{-5}	1×10^{-5}	1×10^{-5}	1×10^{-5}	1×10^{-5}	1×10^{-5}	6×10^{-6}	9×10^{-6}
$E_H(\theta)$	3×10^{-5}	3×10^{-5}	3×10^{-5}	1×10^{-5}	7×10^{-6}	5×10^{-6}	3×10^{-6}	2×10^{-7}	1×10^{-5}	1×10^{-5}	1×10^{-5}
	3×10^{-5}	3×10^{-5}	2×10^{-5}	1×10^{-5}	3×10^{-5}	2×10^{-5}	4×10^{-5}	1×10^{-5}	4×10^{-6}	3×10^{-5}	2×10^{-5}
	1×10^{-3}	1×10^{-3}	1×10^{-3}	8×10^{-4}	8×10^{-4}	8×10^{-4}	6×10^{-4}	3×10^{-4}	1×10^{-4}	5×10^{-4}	4×10^{-4}
$I_H(\theta)$	9×10^{-4}	1×10^{-3}	2×10^{-3}	9×10^{-4}	6×10^{-4}	3×10^{-4}	4×10^{-4}	6×10^{-4}	6×10^{-4}	1×10^{-3}	4×10^{-4}
	1×10^{-3}	7×10^{-4}	4×10^{-5}	1×10^{-3}	5×10^{-4}	1×10^{-3}	4×10^{-4}	5×10^{-5}	3×10^{-4}	1×10^{-4}	8×10^{-5}
	9×10^{-4}	1×10^{-3}	9×10^{-4}	8×10^{-4}	6×10^{-4}	6×10^{-4}	5×10^{-4}	1×10^{-4}	2×10^{-4}	1×10^{-4}	4×10^{-5}
$C_H(\theta)$	4×10^{-5}	3×10^{-4}	2×10^{-4}	1×10^{-4}	1×10^{-4}	2×10^{-4}	3×10^{-4}	5×10^{-4}	2×10^{-4}	1×10^{-4}	9×10^{-4}
	6×10^{-4}	2×10^{-4}	1×10^{-4}	2×10^{-4}	6×10^{-5}	4×10^{-4}	2×10^{-4}	4×10^{-4}	4×10^{-4}	1×10^{-3}	8×10^{-4}
	6×10^{-5}	1×10^{-4}	1×10^{-4}	2×10^{-4}	2×10^{-4}	3×10^{-4}	3×10^{-4}	2×10^{-4}	4×10^{-4}	4×10^{-4}	4×10^{-4}
$R_H(\theta)$	2×10^{-7}	2×10^{-4}	4×10^{-5}	4×10^{-5}	9×10^{-5}	5×10^{-5}	9×10^{-5}	1×10^{-4}	2×10^{-4}	3×10^{-5}	1×10^{-4}
	5×10^{-4}	4×10^{-4}	4×10^{-4}	6×10^{-4}	5×10^{-4}	5×10^{-4}	2×10^{-4}	5×10^{-4}	4×10^{-4}	3×10^{-4}	4×10^{-4}
	3×10^{-3}	2×10^{-3}	2×10^{-3}	2×10^{-3}	9×10^{-3}	1×10^{-3}	7×10^{-3}	9×10^{-6}	1×10^{-3}	2×10^{-3}	4×10^{-3}
$S_R(\theta)$	1×10^{-2}	8×10^{-4}	8×10^{-5}	9×10^{-4}	2×10^{-3}	9×10^{-3}	4×10^{-3}	5×10^{-4}	1×10^{-3}	1×10^{-2}	3×10^{-3}
	5×10^{-3}	1×10^{-2}	8×10^{-5}	1×10^{-2}	2×10^{-3}	3×10^{-3}	5×10^{-4}	2×10^{-3}	7×10^{-5}	1×10^{-2}	2×10^{-3}
	2×10^{-3}	2×10^{-3}	5×10^{-4}	9×10^{-5}	1×10^{-3}	6×10^{-4}	1×10^{-3}	5×10^{-4}	4×10^{-4}	1×10^{-3}	4×10^{-4}
$E_R(\theta)$	4×10^{-3}	9×10^{-4}	2×10^{-3}	7×10^{-4}	1×10^{-3}	1×10^{-3}	1×10^{-3}	2×10^{-3}	1×10^{-3}	5×10^{-3}	2×10^{-3}
	4×10^{-4}	8×10^{-4}	2×10^{-3}	5×10^{-4}	2×10^{-3}	5×10^{-5}	4×10^{-4}	4×10^{-3}	9×10^{-4}	3×10^{-3}	1×10^{-3}
	1×10^{-3}	1×10^{-4}	6×10^{-4}	1×10^{-3}	6×10^{-4}	2×10^{-3}	2×10^{-3}	1×10^{-4}	4×10^{-4}	3×10^{-3}	1×10^{-3}
$I_R(\theta)$	2×10^{-3}	1×10^{-3}	3×10^{-3}	2×10^{-3}	2×10^{-3}	2×10^{-3}	2×10^{-3}	3×10^{-3}	7×10^{-4}	8×10^{-3}	2×10^{-3}
	2×10^{-3}	3×10^{-4}	1×10^{-4}	3×10^{-3}	2×10^{-3}	2×10^{-4}	3×10^{-3}	6×10^{-4}	1×10^{-3}	8×10^{-3}	1×10^{-3}

4. Conclusions

In this work, the numerical performances of the MTS based on the novel stochastic procedure through the radial basis scale conjugate gradient deep neural network have been presented. The nonlinear dynamics of the MTS was divided into rodent and human. The human was further categorized into susceptible, infectious, exposed, clinically ill, and recovered, while the rodent had three groups, i.e., susceptible, infected, and exposed. Some of the conclusions of this work are presented as follows:

- The nonlinear system of differential equations based on the MTS is successfully solved by using the stochastic approaches;
- The deep learning neural network along with the SCG and radial basis is used to present the numerical solutions of the MTS;
- Twelve and twenty neurons in the structure of hidden layers have been used in the deep learning process;
- A dataset was constructed using the Adams method, which is refined further through the process of train, validation, and test by taking 0.15, 0.13 and 0.72 values;
- 850 epochs, activation radial basis function, test performances through MSE and optimization-based SCG were used throughout the process for solving the MTS;

- The exactness of RB-SCGDNN was performed through the comparison of proposed and reference results. Moreover, negligible AE further enhanced the correctness of the scheme.
- The reliability of RB-SCGDNN procedure was verified through different statistical configuration using regression, correlation, ToS, and EHs.

In future, the RB-SCGDNN procedure can be applied to solve different nonlinear systems based on the fluid, fractional order, and other biological models [39–46].

Author Contributions: Investigation, J.L.G.G. and Z.S. writing—original draft preparation, J.L.G.G. and Z.S. Validation, S.B.S. All authors have read and agreed to the published version of the manuscript.

Funding: Technical University of Cartagena, Applied Math 2023-grant.

Acknowledgments: The authors are thankful to UAEU for the financial support through the UPAR grant number 12S002.

Conflicts of Interest: All the authors of the manuscript declared that there are no potential conflicts of interest.

References

1. Arden, M.A.; Chilcot, J. Health psychology and the coronavirus (COVID-19) global pandemic: A call for research. *Br. J. Health Psychol.* **2020**, *25*, 231–232. [CrossRef] [PubMed]
2. Xiang, Y.; White, A. Monkeypox virus emerges from the shadow of its more infamous cousin: Family biology matters. *Emerg. Microbes Infect.* **2022**, *11*, 1768–1777. [CrossRef] [PubMed]
3. Realegeno, S.; Puschnik, A.S.; Kumar, A.; Goldsmith, C.; Burgado, J.; Sambhara, S.; Olson, V.A.; Carroll, D.; Damon, I.; Hirata, T.; et al. Monkeypox Virus Host Factor Screen Using Haploid Cells Identifies Essential Role of GARP Complex in Extracellular Virus Formation. *J. Virol.* **2017**, *91*, e00011-17. [CrossRef] [PubMed]
4. Guarner, J.; del Rio, C.; Malani, P.N. Monkeypox in 2022—What Clinicians Need to Know. *JAMA* **2022**, *328*, 139–140. [CrossRef]
5. Durski, K.N.; McCollum, A.M.; Nakazawa, Y.; Petersen, B.W.; Reynolds, M.G.; Briand, S.; Djingarey, M.H.; Olson, V.; Damon, I.K.; Khalakdina, A. Emergence of monkeypox in West Africa and Central Africa, 1970–2017/Emergence de l'orthopoxvirose simienne en Afrique de l'Ouest et en Afrique centrale, 1970–2017. *Wkly. Epidemiol. Rec.* **2018**, *93*, 125–133.
6. Durski, K.N.; McCollum, A.M.; Nakazawa, Y.; Petersen, B.W.; Reynolds, M.G.; Briand, S.; Djingarey, M.H.; Olson, V.; Damon, I.K.; Khalakdina, A. Emergence of monkeypox—West and central Africa, 1970–2017. *Morb. Mortal. Wkly. Rep.* **2018**, *67*, 306. [CrossRef]
7. Pastula, D.M.; Tyler, K.L. An Overview of Monkeypox Virus and Its Neuroinvasive Potential. *Ann. Neurol.* **2022**, *92*, 527–531. [CrossRef]
8. Paluku, K.; Jezek, Z.; Szczeniowski, M. Human monkeypox: Confusion with chickenpox. *Acta Trop.* **1988**, *45*, 297–307. [CrossRef]
9. Minhaj, F.S.; Ogale, Y.P.; Whitehill, F.; Schultz, J.; Foote, M.; Davidson, W.; Hughes, C.M.; Wilkins, K.; Bachmann, L.; Chatelain, R.; et al. Monkeypox outbreak—Nine states, May 2022. *Morb. Mortal. Wkly. Rep.* **2022**, *71*, 764. [CrossRef]
10. Huhn, G.D.; Bauer, A.M.; Yorita, K.; Graham, M.B.; Sejvar, J.; Likos, A.; Damon, I.K.; Reynolds, M.; Kuehnert, M.J. Clinical Characteristics of Human Monkeypox, and Risk Factors for Severe Disease. *Clin. Infect. Dis.* **2005**, *41*, 1742–1751. [CrossRef]
11. Rizk, J.G.; Lippi, G.; Henry, B.M.; Forthal, D.N.; Rizk, Y. Prevention and treatment of monkeypox. *Drugs* **2022**, *82*, 957–963. [CrossRef] [PubMed]
12. Karan, A.; Styczynski, A.R.; Huang, C.; Sahoo, M.K.; Srinivasan, K.; Pinsky, B.A.; Salinas, J.L. Human Monkeypox without Viral Prodrome or Sexual Exposure, California, USA, 2022. *Emerg. Infect. Dis.* **2022**, *28*, 2121–2123. [CrossRef] [PubMed]
13. Bunge, E.M.; Hoet, B.; Chen, L.; Lienert, F.; Weidenthaler, H.; Baer, L.R.; Steffen, R. The changing epidemiology of human monkeypox—A potential threat? A systematic review. *PLoS Neglected Trop. Dis.* **2022**, *16*, e0010141. [CrossRef] [PubMed]
14. Statistics Sweden. Design Your Questions Right: How to Develop, Test, Evaluate and Improve Questionnaires 2004. Available online: http://www.scb.se/statistik/_publikationer/OV9999_2004A01_BR_X97OP0402.pdf (accessed on 5 June 2020).
15. Nguyen, P.Y.; Ajisegiri, W.S.; Costantino, V.; Chughtai, A.A.; MacIntyre, C.R. Reemergence of human monkeypox and declining population Immunity in the context of urbanization, Nigeria, 2017–2020. *Emerg. Infect. Dis.* **2021**, *27*, 1007. [CrossRef] [PubMed]
16. Alakunle, E.; Moens, U.; Nchinda, G.; Okeke, M. Monkeypox Virus in Nigeria: Infection Biology, Epidemiology, and Evolution. *Viruses* **2020**, *12*, 1257. [CrossRef]
17. Trejos, D.Y.; Valverde, J.C.; Venturino, E. Dynamics of infectious diseases: A review of the main biological aspects and their mathematical translation. *Appl. Math. Nonlinear Sci.* **2022**, *7*, 1–26. [CrossRef]
18. Peter, O.J.; Oguntolu, F.A.; Ojo, M.M.; Oyeniyi, A.O.; Jan, R.; Khan, I. Fractional order mathematical model of monkeypox transmission dynamics. *Phys. Scr.* **2022**, *97*, 084005. [CrossRef]
19. Peter, O.J.; Kumar, S.; Kumari, N.; Oguntolu, F.A.; Oshinubi, K.; Musa, R. Transmission dynamics of Monkeypox virus: A mathematical modelling approach. *Model. Earth Syst. Environ.* **2021**, *8*, 3423–3434. [CrossRef]
20. Ali, A.K. Dynamics of Sofic Shifts. *3C Tecnol. Glosas de Innov. Apl. a la Pyme* **2022**, *11*, 13–23. [CrossRef]
21. Peter, O.J.; Viriyapong, R.; Oguntolu, F.A.; Yosyingyong, P.; Edogbanya, H.O.; Ajisope, M.O. Stability and optimal control analysis of an SCIR epidemic model. *J. Math. Comput. Sci.* **2020**, *10*, 2722–2753. [CrossRef]

22. Ojo, M.M.; Gbadamosi, B.; Olukayode, A.; Oluwaseun, O.R. Sensitivity Analysis of Dengue Model with Saturated Incidence Rate. *Oalib* **2018**, *5*, 1–17. [CrossRef]
23. Ayoola, T.A.; Edogbanya, H.O.; Peter, O.J.; Oguntolu, F.A.; Oshinubi, K.; Olaosebikan, M.L. Modelling and optimal control analysis of typhoid fever. *J. Math. Comput. Sci.* **2021**, *11*, 6666–6682. [CrossRef]
24. Umar, M.; Sabir, Z.; Raja, M.; Shoaib, M.; Gupta, M.; Sánchez, Y. A Stochastic Intelligent Computing with Neuro-Evolution Heuristics for Nonlinear SITR System of Novel COVID-19 Dynamics. *Symmetry* **2020**, *12*, 1628. [CrossRef]
25. Sabir, Z. Stochastic numerical investigations for nonlinear three-species food chain system. *Int. J. Biomath.* **2021**, *15*, 2250005. [CrossRef]
26. Umar, M.; Sabir, Z.; Raja, M.A.Z.; Aguilar, J.G.; Amin, F.; Shoaib, M. Neuro-swarm intelligent computing paradigm for nonlinear HIV infection model with CD4+ T-cells. *Math. Comput. Simul.* **2021**, *188*, 241–253. [CrossRef]
27. Sabir, Z.; Guirao, J.L.; Saeed, T. Solving a novel designed second order nonlinear Lane–Emden delay differential model using the heuristic techniques. *Appl. Soft Comput.* **2021**, *102*, 107105. [CrossRef]
28. Guirao, J.L.; Sabir, Z.; Saeed, T. Design and Numerical Solutions of a Novel Third-Order Nonlinear Emden–Fowler Delay Differential Model. *Math. Probl. Eng.* **2020**, *2020*, 1–9. [CrossRef]
29. Singh, N. Applications of Fixed Point Theorems to Solutions of Operator Equations in Banach Spaces. In *3C TIC Cuadernos de Desarrollo Aplicados a las TIC*; 3ciencias: Alcoy, Spain, 2022; Volume 11, pp. 72–79. [CrossRef]
30. Andrei, N. Scaled conjugate gradient algorithms for unconstrained optimization. *Comput. Optim. Appl.* **2007**, *38*, 401–416. [CrossRef]
31. Yuan, G.; Li, T.; Hu, W. A conjugate gradient algorithm for large-scale nonlinear equations and image restoration problems. *Appl. Numer. Math.* **2019**, *147*, 129–141. [CrossRef]
32. Abubakar, A.B.; Kumam, P.; Malik, M.; Ibrahim, A.H. A hybrid conjugate gradient based approach for solving unconstrained optimization and motion control problems. *Math. Comput. Simul.* **2021**, *201*, 640–657. [CrossRef]
33. Vargas, J.O.; Batista, A.C.; Batista, L.S.; Adriano, R. On the computational complexity of the conjugate-gradient method for solving inverse scattering problems. *J. Electromagn. Waves Appl.* **2021**, *35*, 2323–2334. [CrossRef]
34. Abubakar, A.B.; Kumam, P.; Ibrahim, A.H.; Chaipunya, P.; Rano, S.A. New hybrid three-term spectral-conjugate gradient method for finding solutions of nonlinear monotone operator equations with applications. *Math. Comput. Simul.* **2021**, *201*, 670–683. [CrossRef]
35. Awwal, A.M.; Sulaiman, I.M.; Malik, M.; Mamat, M.; Kumam, P.; Sitthithakerngkiet, K. A Spectral RMIL+ Conjugate Gradient Method for Unconstrained Optimization With Applications in Portfolio Selection and Motion Control. *IEEE Access* **2021**, *9*, 75398–75414. [CrossRef]
36. Chen, Q.; Sabir, Z.; Raja, M.A.Z.; Gao, W.; Baskonus, H.M. A fractional study based on the economic and environmental mathematical model. *Alex. Eng. J.* **2023**, *65*, 761–770. [CrossRef]
37. Sada, S.O. Improving the predictive accuracy of artificial neural network (ANN) approach in a mild steel turning operation. *Int. J. Adv. Manuf. Technol.* **2021**, *112*, 2389–2398. [CrossRef]
38. Khodadadian, A.; Parvizi, M.; Teshnehlab, M.; Heitzinger, C. Rational Design of Field-Effect Sensors Using Partial Differ-ential Equations, Bayesian Inversion, and Artificial Neural Networks. *Sensors* **2022**, *22*, 4785. [CrossRef]
39. Sun, C.; Li, H. Algebraic Formulation and Application of Multi-Input Single-Output Hierarchical Fuzzy Systems with Correction Factors. *IEEE Trans. Fuzzy Syst.* 2022; *Early Access*. [CrossRef]
40. Sun, C.; Li, H. Parallel fuzzy relation matrix factorization towards algebraic formulation, universal approximation and interpretability of MIMO hierarchical fuzzy systems. *Fuzzy Sets Syst.* **2022**, *450*, 68–86. [CrossRef]
41. Durur, H.; Yokuş, A. Exact solutions of (2 + 1)-Ablowitz-Kaup-Newell-Segur equation. *Appl. Math. Nonlinear Sci.* **2020**, *6*, 381–386. [CrossRef]
42. Sulaiman, T.A.; Bulut, H.; Baskonus, H.M. On the exact solutions to some system of complex nonlinear models. *Appl. Math. Nonlinear Sci.* **2020**, *6*, 29–42. [CrossRef]
43. Gençoğlu, M.T.; Agarwal, P. Use of Quantum Differential Equations in Sonic Processes. *Appl. Math. Nonlinear Sci.* **2020**, *6*, 21–28. [CrossRef]
44. Aghili, A. Complete Solution for the Time Fractional Diffusion Problem with Mixed Boundary Conditions by Operational Method. *Appl. Math. Nonlinear Sci.* **2020**, *6*, 9–20. [CrossRef]
45. Rahaman, H.; Hasan, M.K.; Ali, A.; Alam, M.S. Implicit Methods for Numerical Solution of Singular Initial Value Problems. *Appl. Math. Nonlinear Sci.* **2020**, *6*, 1–8. [CrossRef]
46. İlhan, E.; Kıymaz, I.O. A generalization of truncated M-fractional derivative and applications to fractional differential equations. *Appl. Math. Nonlinear Sci.* **2020**, *5*, 171–188.